



# Wavelet analysis of the magnetotail response to solar wind fluctuations during HILDCCA events

Adriane Marques de Souza Franco<sup>1</sup>, Ezequiel Echer<sup>1</sup>, Mauricio José Alves Bolzan<sup>2</sup>

<sup>1</sup>Division of Space Geophysics, National Institute for Space Research (INPE), São José dos Campos, 12227-010, Brazil

<sup>2</sup>Astronomy and Space Physics Laboratory, Federal University of Jataí, Jataí, 75801-615, Brazil

*Correspondence to:* Adrie M. S. Franco (adrianemarquesds@gmail.com)

**Abstract.** In this work a study of the effects of the High-Intensity Long-Duration Continuous AE activity events (HILDCAAs) in the magnetotail was conducted. The aim of this study was to search the main frequencies during HILDCAAs in the Bx component of the geomagnetic field, as well as at the main frequencies which the magnetotail responds to the solar wind during these events. In order to conduct this analysis the wavelet transform was employed HILDCAA events that occurred after the Cluster mission (2000) and coincided with the Cluster crossing through the tail of the magnetosphere from 2003 to 2007. Altogether, 25 most energetic periods were observed, which 76% are  $\leq 4$  hours. The cross wavelet analysis technique was also used for the development of this study. It was applied to data of the Bz-IMF component and the Bx geomagnetic component, searching to obtain the periods in that had the highest correlation between these two series. To obtain these periods is important to identify frequencies on which the coupling of energy is stronger, as well the modulation of the magnetotail by the solar wind during HILDCAA events. The majority of correlation periods between the Bz (IMF) and Bx component of the geomagnetic field observed also were  $\leq 4$  hours, with 62.9% of the periods. Thus the magnetotail responds stronger to IMF fluctuations during HILDCCAS at 2-4 hours scales, which are typical substorm periods.

## 1 Introduction

The perturbations that occur in the Earth's magnetic field due to interaction with the solar wind are called magnetic activity. The most known types of magnetic activities are the geomagnetic storms, magnetic substorms and HILDCAAs (High-intensity long-duration continuous AE activity) (Tsurutani and Gonzalez, 1987; Gonzalez et al., 1994). HILDCAA event is a kind of auroral activity and its cause is associated with the southward Interplanetary Magnetic Field (IMF)  $B_z$  component of Alfvén waves (Tsurutani and Gonzalez, 1987; Tsurutani et al., 2004). These events are defined by four criteria: (i) AE index has to present at least one peak value  $\geq 1000$  nT, (ii) the event must last for a minimum of 2 days, (iii) the AE index cannot drop below 200 nT for more than 2 hours at a time, and (iv) the event cannot occurs during the main phase of a geomagnetic storm.



In the first studies were done about HILDCAAs, the question if these events could be a kind of continuous substorms arose. Tsurutani et al. (2004) proved the opposite, since substorms do not have relation with high values of AE index, which is observed during HILDCAA events. Another characteristic of HILDCAAs that distinguishes from substorms is the aurora formed by these events. During HILDCAA events the auroras are weak or moderate, distributed in the whole auroral zone, 5 and can last several days, while during substorms, auroras are confined in small regions and lasts 15 minutes (Guarnieri, 2006).

HILDCAAs are events of low intensity, when compared with geomagnetic storms. However, the integrated energy during the whole duration of a HILDCAA event can be bigger than the energy of moderate geomagnetic storms (Guarnieri, 2005).

Recent studies of the energy transfer from solar wind to the magnetosphere/ionosphere during HILDCAAs have shown that

10 two mechanisms are responsible for the energy and matter transfer, namely the magnetic reconnection (Dungey, 1961) and viscous interaction (Axford and Hines, 1961; Mendes et al., 2017). Vira et al. (2014) have shown the main process of solar wind energy dissipation in the magnetosphere during HILDCAA is by Joule heating in the auroral region, with 67% of the input energy. It was seen that the coupling between solar wind and the magnetosphere during these events occurs mainly in 15 periods  $\leq 8$  hours (Souza et al., 2018). Similar periods were observed as most energetic periods in AE index and Bz interplanetary magnetic field (IMF) component. Those are comparable to the periods observed in the interplanetary Alfvén waves present in High-Speed Streams (HSS) (Smith et al., 1995; Souza et al., 2016).

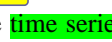
The magnetotail has an important role in the energy transfer from solar wind to the inner magnetosphere, since the energy of this process is stored in the tail (Lopez, 1990). During geomagnetic substorms, the solar wind energy is stored in the magnetotail during the initial phase and then in the expansion phase is suddenly released and deposited in the ionosphere 20 (Akasofu, 2013). Its storage can be interpreted as asymmetric ring current and magnetotail currents which respond to the periods of substorms that were observed as 2-4 hours (Tianov et al., 2001). The aim of this work is to identify the main periodicities of HILDCAA events in the geomagnetic field Bx component in the magnetotail and also to study at which periods the energy is preferentially transferred from the solar wind to that region during these activities using wavelet analyses.

## 25 2 Data

In order to develop this study, geomagnetic field Bx component data obtained by the satellite SC4 of the Cluster constellation were used. The events were selected (one in August 2003, two in September 2003, one in October 2003, one in September 2004 one in August 2005, two in October 2006 and one in September 2007), which correspond to the events when Cluster crossed the plasma sheet during the occurrence of HILDCAAs. In this analysis AE and IMF Bz component 30 data were also used. The AE indices at 1 min time resolution were obtained from the World Data Center for Geomagnetism, Kyoto, Japan (<http://wdc.kugi.kyoto-u.ac.jp/>), and the Bz IMF data (1 min) were obtained from the OMNI web (<http://omniweb.gsfc.nasa.gov/>).



Table 1 shows some relevant information about the HILDCAA events that were analyzed, where the start and end time  each event is  given, as well as the data intervals analyzed for the Cluster magnetotail crossings.

In Figure 1 the time series  during the HILDCAA event that occurred between 03:38 UT, October 15 to 18:35 UT, October 22, 2003 (event 4 in Table 1) are shown. The upper panel shows the IMF Bz component, the middle panel the AE index, and the bottom panel the Cluster tail Bx component. From this Figure it is possible to observe HILDCAA features in the Bz IMF and AE index data, where Alfvénic fluctuations can be observed in the IMF Bz data. In the AE, the values of the index can  reach  peaks higher than 1000 nT. The interval on which the Cluster crossed the magnetotail during the event is marked with the red rectangle on the panels.

The intervals of the Cluster crossings the magnetotail during HILDCAAs selected for our study were identified by analyzing the orbit of the spacecraft during the HILDCAA events, where these nine events were obtained. The Cluster orbit in the XZ plane for the HILDCAA plotted in Figure 1 is shown in Figure 2, where the Cluster magnetotail crossing is marked in  on the orbit panel.

### 3 Methodology

Non-stationary time series can be analyzed by wavelet transform, a powerful mathematical tool that is able to show the temporal variability of the power spectral density (Morettin, 1992). Wavelet functions  $\psi(t)$  are generated by a simple function called wavelet-mother  Equation 1, which suffers expansion  $\psi(t) \rightarrow \psi(2t)$ , and translations  $\psi(t) \rightarrow \psi(t + 1)$  in time, giving rise to those wavelet functions, well known as wavelet-daughters (Torrence and Compo, 1998).

$$\psi_{a,b}(t) = \frac{1}{\sqrt{a}} \psi\left(\frac{t-b}{a}\right), \quad (1)$$

20

where  $a$  represents the scale associated to the expansion and contraction of the wavelet, and  $b$  is the temporal location, which relates to the translation in time.

The Wavelet Transform (WT) applied on  $f(t)$  time series is defined as :

$$25 \quad TW(a, b) = \int f(x) \psi_{a,b}^*(t) dt, \quad (2)$$

where  $f(x)$  is the time series,  $\psi_{a,b}(t)$  is the wavelet function and  $\psi_{a,b}^*(t)$  represents the complex conjugate thereof.

The wavelet function can be characterized  two types of functions, the continuous and discrete ones (Daubechies, 1992). The discrete wavelets are used for decomposition of time series in frequency, which is useful for filtering process. 30 Among the most known functions are the Meyer, Daubechies and Haar (Grinsted et al., 2004). The continuous wavelet functions allow the separation of phase and amplitude components associated with the signal, and then they are generally



used for analysis of the continuous wavelet transform. The most common continuous wavelet functions are the Mexican Hat and the Morlet functions (Torrence and Compo 1998; Addison, 2018). In this paper, a discrete and a complex wavelet function were used, the Haar function in order to remove long term trends in the data and the Morlet function for the periodicity identification.

5 As Cluster spacecraft travels through large spatial and **latitudes**, where the Earth's magnetic field has strong dependence, **it samples** have large spatial variations. These are noted in time as long term trend, as it can be observed in the bottom panel of Figure 1, in the geomagnetic Bx component. These long trends observed in the geomagnetic field Bx component data can affect the results of the periodicities identified by wavelet analysis. In order to remove it, a technique of long-term trend extraction using Haar wavelet function was applied in the data. The Haar wavelet function is the simplest  
 10 type of wavelet and is used since 1910 (Haar, 1910; Porwik and Lisowska, 2004). The Haar function is defined as a complete orthogonal system of functions which have a dyadic dilatation  $a = 2^j$  and with translations in discrete steps ( $b = 2^{-j}k$ ) (Porwik and Lisowska, 2004; Bolzan et al., 2009; Bolzan et al., 2019). The Haar wavelet function is shown in Equation 3

$$\Psi_{j,k}(t) = \begin{cases} 2^{\frac{j}{2}}, & 2^{-j}k \leq t < 2^{-j}\left(k + \frac{1}{2}\right) \\ -2^{\frac{j}{2}}, & 2^{-j}\left(k + \frac{1}{2}\right) \leq t < 2^{-j}(k + 1) \\ 0, & \text{otherwise} \end{cases} \quad 3$$

where  $j$  and  $k$  are integers.

15 The long-term trend extraction method consists to apply Haar wavelet function in the data, which decompose it in dyadic scales, after identifying the scales where the long-term periodicities are present; these scales are removed of the data, in such a way that the main characteristics of the time series are maintained (Bolzan et al., 2019). Figure 3 shows an example where this technique was applied in the geomagnetic field Bx component in the magnetotail during a **HILDCAA event that occurred from 22:19 UT, August 5 to 22:54 UT, August 7, 2005**. The upper panel shows the original time series where the  
 20 long trend can be observed, and the bottom panel shows the time series after filtering the scales, and removing the long-term trend. As the wavelet mechanism of decomposition is in dyadic scales, when we remove the frequencies where the long trend appears, a number of points are removed from the data time series. However, it does not affect the time scales of the signal because it is possible to observe that all structures presented in the time series are located in the same time before and after the filtering process. Due the dyadic process of the filtering, the last of the time period of the time series is lost, as  
 25 observed in Figure 3. However, these loss of the some data points do not affect the results **here obtained** because we **are** focus the global phenomena and not particularly inside the time series.

After removing the long tendency in the data, the Morlet wavelet was applied with the aim to identify the main periodicities present **on it**. The Morlet wavelet is a plane wave modulated by a Gaussian envelope and can be described by equation 4 (Torrence e Compo, 1998):

30

$$\psi(t) = e^{i\xi_0 t} e^{\frac{-t^2}{2}}, \quad 4$$



$\xi_0$  represents the dimensionless frequency. In this work this parameter was used as 6.0 since its shape gives good localization in time.

The Global Wavelet Spectrum (GWS) shows the integrated energy in time for each frequency. Consequently, the GWS is useful for the identification of the most energetic frequencies/periods in a time series. The GWS is given as:

5

$$GWS = \int |TW(a, b)|^2 db, \quad (5)$$

This study has also the aim to identify the periods on which the energy transfer from the solar wind and auroral region to the magnetotail more efficient during HILDCAA events. In order to obtain that, the Cross-Wavelet Transform (CWT) was

10 used. The TWC (Equation 6) is constructed from two continuous WT of two time series, which allows analyzing the correlation between the time series as function of the signal period and its temporal evolution identifying their power in common (Grinsted et al., 2004; Bolzan et al., 2012).

$$W^{yx}(a, b) = W^x(a, b)W^y(a, b)^*, \quad (6)$$

15

Where  $W^x$  and  $W^y$  represent the WT applied to the time series x(t) and y(t), and (\*) represents the complex conjugate of the WT.

In order to study the main periods with higher correlation between two time series the Global Correlation Spectrum (GCS) is computed. The GCS can be obtained rewriting Equation 5 as:

20

$$GCS = \frac{\sigma^x \sigma^y}{\sigma^x + \sigma^y} \int |W^{xy}(a, b)|^2 db, \quad (7)$$

Where  $\sigma^x$  and  $\sigma^y$  represent the variances of the time series x(t) and y(t), respectively.

## 4 Results

25 After removing the long trend of the data, the WT was applied on them in order to identify the main periodicities in the geomagnetic Bx component. Figure 4 shows the WT applied to the Bx geomagnetic component during the HILDCAA event that occurred from 22:19 UT, August 5 to 22:54 UT, August 7, 2005, for the last 23 hours of the event, period during which the Cluster crossed the magnetotail (same interval of Figure 3). Figure 4-a) shows the Bx filtered time series, Figure 4-b) the wavelet power spectrum and Figure 4-c) shows the 3 most energetic periods present in the data, the first at 1.1h, second at 30 2.3 h and the last at 4.3h.



With the goal of identifying the main periods of Bx geomagnetic component, the periods with peaks of energy found in the GWS plots in all events were divided in ranges of 2 hours. A total of 25 periods between 0 and 8 hours were identified and the result of this analysis is shown in the histogram of Figure 5.

All periods here noted in geomagnetic Bx component were found in the same range observed by Souza et al., (2016) for the 5 most energetic periods in IMF Bz component, using 52 HILDCAAs that occurred between 1995 and 2011.

From Figure 5 it is possible to note the most energetic periods were shorter or equal 8 hours. It was observed that 76% of the 25 periods identified occurred in the interval  $\leq 4$  hours. Although it was used a few events for this study, it is worth to say that it corresponds to periods obtained by Borovsky et al. (1993) in a study of the time interval between substorm onsets, where a major period of 2.75 hours was identified. Lee et al. (2006) also observed that repetitive substorms caused by 10 Alfvénic waves in the IMF during high speed stream (HSS) have periods of 1-4 hours. Similar results were also found by Korth et al. in 2006 in the study of events of HSS, wherein substorms were observed with periods between 2 to 4 hours. Also, Bolzan et al. (2012) had found similar periods, 2.3 hours, during corotating interaction regions (CIR) driven storms. As well as Echer et al. (2017) had found periods from 1.8 up to 3.1 h in a study of HSS driven geomagnetic activity events.

The energy distribution in the main periods observed in the geomagnetic Bx component during HILDCAA was studied using 15 the classification introduced by Souza et al., (2016). The energy distribution can be classified in 4 forms: Local, intermittent, Quasi-continuous and continuous. Local classification is characterized by distribution of energy which occurred in only one intense region during the event. In Intermittent distribution one can observe the presence of energy in small regions located in time, but scattered at various moments during the event. In Quasi-continuous distribution, the range of periods with intense energy can be observed in almost the whole event. And in Continuous, a range of energy can be observed in the 20 whole event. For this study we also count the number of the most energetic periods which fit in each classification and then, a table with the percentage of each behavior was generated and presented (Table 2).

The results showed in Table 2 indicate that the energy distribution presented majority the continuous form during the HILDCAAs, present in 32% of the 25 periods observed inside the influence cone. Note that 52% of the periods are quasi-continuous or intermittent, which means transient events, which is a characteristic of substorms (Hones Jr., 1979).

25

#### 4.1 Correlation between IMF Bz and Bx geomagnetic

The cross wavelet transform (XWT) is applied to the data of IMF Bz component (GSM) and the Bx geomagnetic component, in order to search periods with largest correlation between these two time series. To obtain these periods is important to identify the frequencies on which the coupling of energy is stronger, as well the modulation of the magnetotail 30 by the solar wind during HILDCAA events (Korth et al., 2006; Bolzan et al., 2012). The classification of the characteristic form of the periods with higher correlations obtained by the XWT also was done.

The XWT of the HILDCAA which occurred from 15:11UT, August 20 to 15:43 UT, August 24, 2003 (first event in Table 1) is presented in Figure 6. Figure 6.a) shows the time series of Bz IMF component and Bx geomagnetic component time



series, b) the XWT between those two time series, and c) the global cross wavelet spectrum. In the Figure 6-c) it is possible to observe three periods with higher values of correlations, related to the regions characterized as intermittent, local and quasi-continuous, respectively, in Figure 6-b). The first peak of correlation has period of 1.2 h, the second at 3.2 hours, and the last one, at 5.7 hours.

5 A total of 27 periods of higher correlation was identified between Bz-IMF (GSM) and the Bx geomagnetic component observed in these nine HILDCAA events. These periods were also divided in ranges of 2 hours and the percentage of the number of periods identified in each interval is presented in the histogram of Figure 7. Through Figure 7, it is possible to see that the energy transfer is more efficient for periods  $\leq$  4 hours, which presented 62.9% of the signals with higher correlation. This interval corresponds to the periods observed by Echer et al., 2017 during HSS for the intervals from 19-20 September  
10 and 15 to 16 October 2003. In that work periods from 1.8 up to 3.1 h were found in the cross wavelet analysis between ACE IMF Bz component and Cluster tail Bx geomagnetic component. The periods analyzed by Echer et al., 2017 include the HILDCAA events number 2 and 3 listed in Table 1.

The correlation distribution form was also classified with the criteria used in the energy distribution of the Bx geomagnetic component. The result of this study is shown in Table 3. From the 27 periods of higher correlation, 4 periods have not  
15 presented a clear behavior and they were not included in the classification analysis. The local distribution was the most observed here, present in 43.5% of the periods with higher correlation obtained. These results show that in ~~this this~~ study, more than 95% of coupling between IMF Bz component and geomagnetic magnetotail Bx component is non continuous. Again, it shows the typical substorm intermittent behavior.

#### 4.2 Energy transfer from magnetotail to auroral region during HILDCAA events

20 With the aim ~~of to~~ to verify at which frequencies the transfer of the magnetotail stored energy to the auroral region occurs during HILDCAAs, as it was observed before for other kinds of geomagnetic activities, as substorms (Hargreaves, 1992), the CWT was applied between the Bx geomagnetic tail component and the AE index. Figure 8 shows the CWT applied ~~in one of the 9 events, which corresponds to~~ event 1 from Table 1. In Figure 8-a) Bx and AE time series are ~~observed~~. In Figure 8-b)  
25 the CWT can be observed. By Figure 8-b) it is possible to note that there is a ~~high intensity of correlation~~ some periods, one of them for almost the whole event. The type of distributions of the correlation is also shown in the figure, which is local and quasi-continuous. In the global correlation spectrum, presented in Figure 8-c), two peaks of the periods of high values of correlation are observed at 3.7 h and at 5.6 hours, respectively.

~~This~~ analysis was also done for the whole data set and a histogram with the periods of high correlation was built, as ~~it~~ shown in Figure 9. By this histogram it is possible to observe that the major periods of correlation are  $\leq$  12 hours. Those  
30 were divided in 6 intervals of 2 hours. Among them, one can notice that the high correlation occurs in periods between 2 and 4 hours, since 45 % of the 20 periods identified are in this range. This result is interesting and means that the energy transfer from the magnetotail to the auroral regions occurs mainly during fluctuations with periods between 2 and 4 hours.



The classification of the correlation distribution was done following the steps of the analysis described previously. By this analysis, the most common correlation distribution types observed was local, present in 55% of the main periods. This result can be seen in Table 4.

In this study the main periodicities in the Bx magnetotail component and also the periodicities at which there were of higher correlation between IMF Bz component and Bx geomagnetic tail component, and between Bx geomagnetic tail component and AE index were determined. This analysis provides the frequencies where stronger energy coupling and modulation of the magnetotail by the IMF Bz variations during HILDCAAs can be observed. The periods that were found in our results agrees with what were found by other authors (Lee et al., 2006; Korth et al., 2006; Bolzan et al., 2012; Echer et al., 2017), where periods of  $\leq 4$  hours were identified, these periods can be associated with quasi-periodic response among these 10 regions, magnetotail and auroral regions, during HILDCAA events, where multiple energy injection in the magnetosphere occur, as it was observed in the energy distribution analysis.

## 5 Conclusion

This paper had as its main goal to identify the main periods of HILDCAA events in the magnetotail, as well as to find the periods of energy transfer from solar wind to the magnetotail and also from magnetotail to the auroral region. The main 15 results obtained here were:

- Most energetic periods were observed for  $T \leq 4$  hours in the Bx component in the magnetotail during HILDCAAS. This result is coincident with cyclic substorm periods observed by Korth et al., 2006.
- The characteristic periods of energy transfer from solar wind to the magnetotail observed in the CWT were also observed mainly for  $\leq 4$  hours, with 62.9% of the identified periods. Echer et al., 2017 also found similar periods in the study of periods of HSS storm and substorm driven events in the magnetotail.
- The energy transfer process between magnetotail and auroral region during HILDCAA events also have shown to be more efficient in periods between 2 and 4 hours, with 45% of the periods identified using CWT analysis. The correlation between the Bx geomagnetic component and the AE index is higher for the local type of distribution, which means that the energy transfer should occurs in local regions in the magnetotail.

25 As conclusion, this work presented some characteristics of HILDCAA events in the magnetotail. The results were shown to be comparable to which was found by other authors studying substorm and HSS storm driven events, which are related to HILDCAA occurrence. Thus the magnetotail responds stronger to IMF fluctuations during HILDCAAS at 2-4 Hours scales, which are typical substorms periods.



## References

Addison, P. S.: Introduction to redundancy rules: the continuous wavelet transform comes of age. *Phil. Trans. R. Soc. A* 376: 20170258. <http://dx.doi.org/10.1098/rsta.2017.0258>, 2018.

Akasofu, S.-I.: The relationship between the magnetosphere and magnetospheric/auroral substorms. *Annales Geophysicae*, 5 31, 387-394, 2013.

Bolzam, M. J. A., Guarnieri, L. F., Vieira, P. C.: Comparisons between two wavelet functions in extracting coherent structures from solar wind time series. *Brazilian Journal of Physics*, 39, 14-17, 2009.

Axford, W.I.; Hines, C.O.: A unifying theory of high latitude geophysical phenomena and geomagnetic storms. *Canadian Journal of Physics*, 39, 10, 1433-146, 1961.

10 Bolzam, M. J. A.; Echer, E.; Korth, A.: Cross-wavelet analysis on the interplanetary and magnetospheric tail magnetic field data. 2012. In: *Congresso Nacional de Matemática Aplicada e Computacional (SBMAC)*, 34., 2012, Águas de Lindóia, São Paulo.

Daubechies, I.: Ten lectures on wavelets. IN: Series: *Cbms-Nsf Regional Conference Series In Applied Mathematics*, 61, Philadelphia. Proceedings... ISBN0898712742, 1992.

15 Dungey, J. W.: Interplanetary magnetic field and the auroral zones. *Phys. Rev. Lett.*, 6, 47-49, 1961.

Echer, E.; Korth, A.; Bolzan, M. J. A.; Friedel, R. H. W.: Global geomagnetic responses to the IMF B<sub>z</sub> fluctuations during the September/October 2003 high-speed stream intervals. *Annales Geophysicae*, 35, 853-868, 2017.

Gonzalez, W. D.; Joselyn, J. A.; Kamide, Y.; Kroehl, H. W.; Rostoker, G.; Tsurutani, B. T.; Vasyliunas, V. M.: what is a geomagnetic storm? *Journal of Geophysical Research*, 99, A4, 5771-5792, 1994.

20 Grinsted, A.; Moore, J. C.; Jevrejeva, S.: Application of the cross wavelet transform and wavelet coherence to geophysical time series. *Nonlinear Processes in Geophysics*, 11, 561-566, 2004.

Guarnieri, F. L.: Estudo da origem interplanetária e solar de eventos de atividade auroral contínua e de longa duração. 316 p. (INPE-13604-TDI/1043). Doctoral Thesis- National Institute for Space Research, São José dos Campos, 2005.

Guarnieri, F. L.: The nature of auroras during high-intensity long-duration continuous AE activity (HILDCAA) events, 1998 to 2001. In: Tsurutani, B. T., McPherron, R. L., Gonzalez, W. D., Lu, G., Sobral, J. H. A.; Gopalswamy, N. (eds.). *Recurrent magnetic storms: corotating solar wind streams*, geophys. monogr., Washington, DC: Am. Geophys. Univ. Press., 167, 235, 2006.

Haar A.: Zur Theorie der orthogonalen Funktionensysteme. *Mathematische Annalen*, 69, 331-371, 1910.

Hajra, R.; Echer, E.; Tsurutani, B. T.; Gonzalez, W.D.: Solarwind-magnetosphere energy coupling efficiency and partitioning: HILDCAAs and preceding CIR storms during solar cycle 23. *Journal of Geophysical Research*, 119, 2675-2690, 2014.

Hargreaves, J. K.: *Solar-terrestrial environment an introduction to geospace - the science of the terrestrial upper atmosphere, ionosphere and magnetosphere* - Cambridge, UK : Cambridge University, 1992.



Hones Jr.: Transient Phenomena in the Magnetotail and their Relation to Substorms. *Space Sciente Reviews*, 23, 393-410, 1979.

Korth, A.; Echer, E.; Guarneri, F. L.; Franz, M.; Friedel, R.; Gonzalez, W. D.; Mouikis, C. G.; Reme: Cluster observations of plasma sheet activity during the September 14-28, 2003 corotating high speed stream event. In: *International Conference 5 On Substorms (Ics-8)*, 8., Alberta. Proceedings... Alberta: Syrjäsuo, and E. Donovan, University of Calgary. 133-138, 2006.

Lee, D.Y.; Lyons, L. R.; Kim, K. C.; Baek, J. H.; Kim, K. H.; Kim, H.J.; Weygand, I. J.; Moon, Y. J.; Cho, K.S.; Park, Y. D.; Han, W.: Repetitive sub storms caused by Alfvénic waves of the interplanetary magnetic field during high - speed solar wind streams. *Journal of Geophysical Research*. 111, 1-14, 2006.

Lopes, R.: Magnetospheric substorms. *Johns Hopkins APL Technical Digest*. 11, 264-271, 1990.

10 Mendes, O.; Domingues, M. O.; Echer, E.; Hajra, R.; Menconi, V.: Characterization of high-intensity, long-duration continuous activity (HILDCAA) events using recurrence quantification analysis.. *Nonlinear Processes in Geophysics*, European Geosciences Union (EGU), 24, 407-417, 2017.

Morettin, P. A.: Ondas e ondeletas: da análise de fourier à análise de ondeletas. São Paulo: Edusp, 296 p, 1992.

Porwik, P.; Lisowska, A.: The Haar–Wavelet Transform in Digital Image Processing: Its Status and Achievements. *Machine 15 Graphics & Vision*, 13, 79-98 2004.

Smith E. J.; Balogh, A.; Neugebauer, M.; Mccomas, D.: Ulysses observations of Alfvén waves in the southen and northern solar hemispheres. *Geophys. Res. Lett.*, 22, 3381-3384, 1995.

Souza, A. M.; Echer, E.; Bolzan, M. J. A.; Hajra, R.: A study on the main periodicities in interplanetary magnetic field Bz component and geomagnetic AE index during HILDCAA events using wavelet analysis. *Journal of Atmospheric and Solar- 20 Terrestrial Physics*, 149, 81–86, 2016.

Souza, A. M.; Echer, E.; Bolzan, M. J. A.; Hajra, R.: Cross-correlation and cross-wavelet analyses of the solar wind IMF Bz and auroral electrojet index AE coupling during HILDCAAs. *Ann. Geophys.*, 36, 205-211, 2018.

Sitnov, M. I.; Sharma, A. S.; Papadopoulos, K.; Vassiliadis, D.: Modeling substorm dynamics of the magnetosphere: from self-organization and self-organized criticality to nonequilibrium phase transitions. *Physical Review E*, 65, 016116, 2001.

25 Torrence, C.; Compo, G. P.: A practical guide to wavelet analysis. *Bulletin of the American Meteorological Society*. 79, 1, 61-78, 1998.

Tsurutani, B. T.; Gonzalez, W. D.: The Cause Of High-Intensity Long- Duration Continuous AE Activity (Hildcaas): Interplanetary Alfvén Wave Trains. *Planet. Space Sci.*, 35, 4, 405-412, 1987.

Tsurutani B. T.; Gonzalez, W. D.; Guarneri, F.L.; Kamide, Y.; Zhou, X.; Arballo, J. K.: Are high-intensity long-duration 30 continuous AE activity (HILDCAA) events substorm expansion events? *Journal of Atmospheric and Solar-Terrestrial Physics*, 66, 67–176, 2004.



## FIGURE CAPTIONS

Figure 1-Time series of IMF Bz (upper panel), AE index (middle panel) and Cluster Bx (bottom panel) for the HILDCAA event that occurred from 03:38 UT, October 15 to 18:35 UT, October 22, 2003.

5

Figure 2- Cluster orbit in the XZ plane for the HILDCAA that occurred from 03:38 UT, October 15 to 18:35 UT, October 22, 2003 (event number 4 in Table 1). The axes are plotted in Earth radii. The marked red line represents the interval on which the Cluster crossed the magnetotail during the event.

10 Figure 3- Geomagnetic field Bx component data for the interval that the Cluster was in the magnetotail during the HILDCAA event that occurred between 22:19 UT, August 5 to 22:54 UT, August 7, 2005. The upper panel shows the original data and the bottom panel shows the detrended data after removal the long tendency.

15 Figure 4- a) Geomagnetic magnetotail field Bx component time series for the interval that the Cluster remained in the magnetotail during the HILDCCA event that occurred between 22:19 UT, August 5 and 22:54 UT, August 7, 2005. b) Wavelet power spectrum. c) GWS.

Figure 5- Histogram of the percentage of the main frequencies in Bx geomagnetic field component in the magnetotail during HILDCAAs.

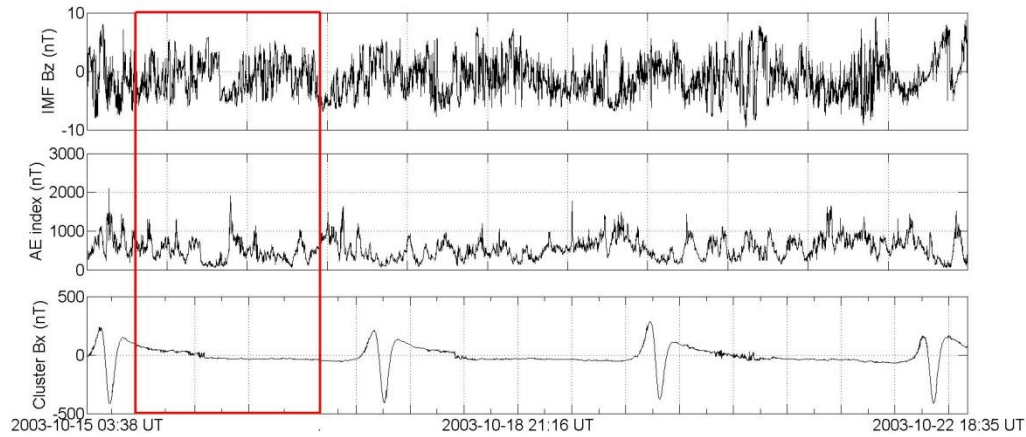
20

Figure-6-a) IMF Bz and Bx geomagnetic field time series. b) Cross wavelet spectrum. c) Global Correlation Spectrum.

Figure 7- Histogram with the periods of highest correlations between Bz IMF component and Bx geomagnetic component.

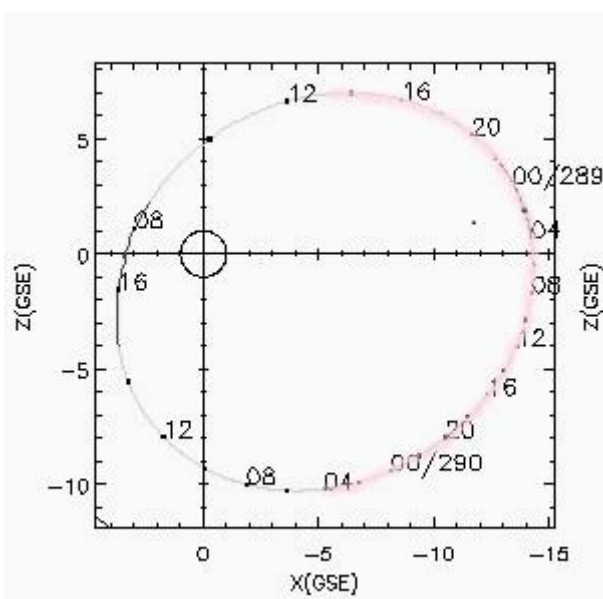
25 Figure 8- a) Bx geomagnetic magnetotail component and AE index time series; b) CWT for the HILDCAA event that occurred between 15:11 UT August, 20 and 15:43 UT August, 24, 2003. c) Global Correlation Spectrum.

Figure 9- Histogram with the periods of high correlation between Bx tail component and the AE index.



**Figure 1.** Time series of IMF Bz (upper panel), AE index (middle panel) and Cluster Bx (bottom panel) for the HILDCAA event that occurred from 03:38 UT, October 15 to 18:35 UT, October 22, 2003.

5



**Figure 2** Cluster orbit in the XZ plane for the HILDCAA that occurred from 03:38 UT, October 15 to 18:35 UT, October 22, 2003 (event number 4 in Table 1). The axes are plotted in Earth radii. The marked read line represents the interval on which the Cluster crossed the magnetotail during the event.

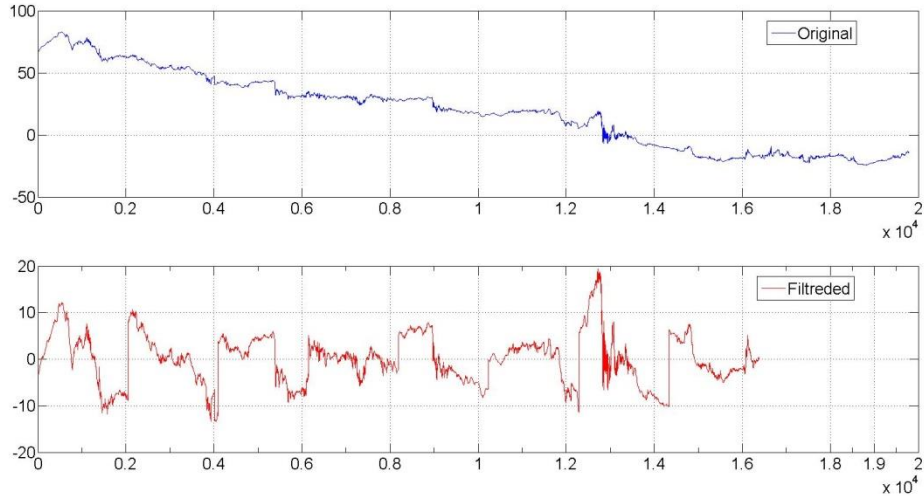


**Figure 3** Geomagnetic field Bx component data for the interval that the Cluster was in the magnetotail during the HILDCAA event that occurred between 22:19 UT, August 5 to 22:54 UT, August 7, 2005. The upper panel shows the original data and the bottom panel shows the detrended data after removal the long tendency.

5

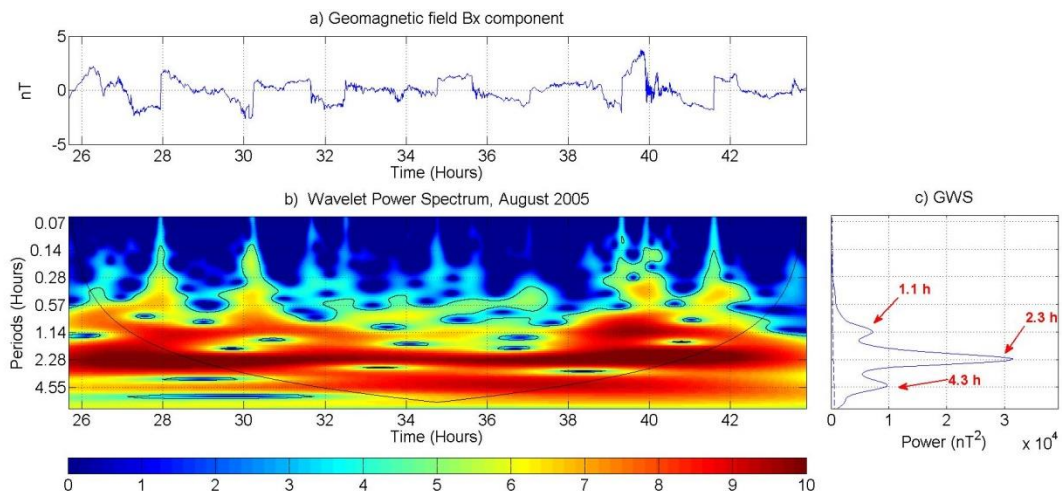


**Figure 4-** a) Geomagnetic magnetotail field Bx component time series the interval that the Cluster remained in the magnetotail during the HILDCAA event that occurred between 22:19 UT, August 5 and 22:54 UT, August 7, 2005. b) Wavelet power spectrum. c) GWS.

10

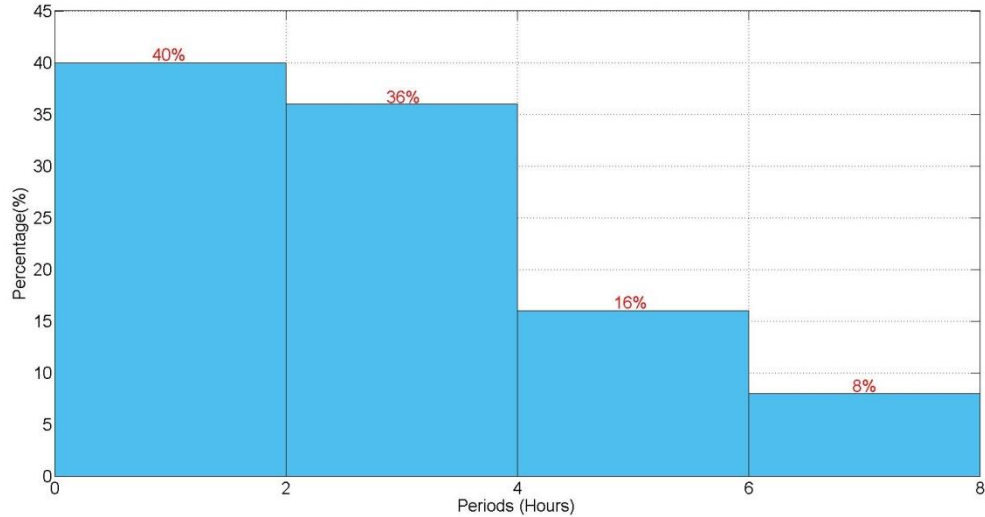


**Figure 5** Histogram of the percentage of the main frequencies in Bx geomagnetic field component in the magnetotail during HILDCAAs.

5

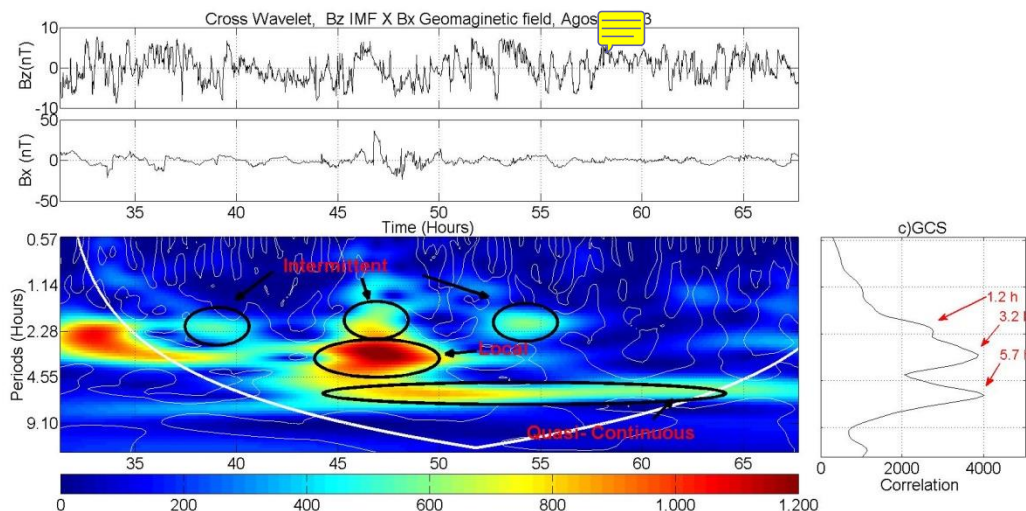


**Figure 6-a)** Bz IMF and Bx geomagnetic field time series. **b)** Cross wavelet spectrum. **c)** Global Correlation Spectrum.

10

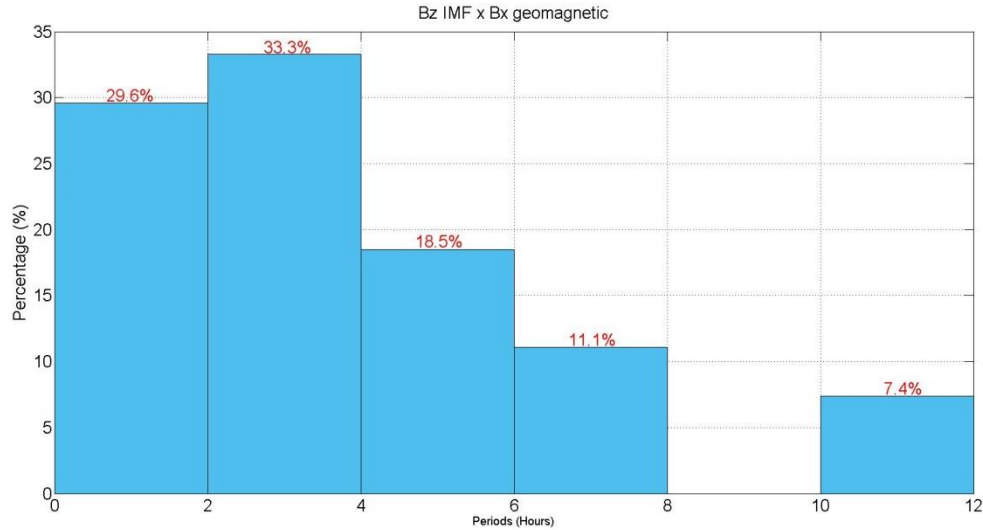
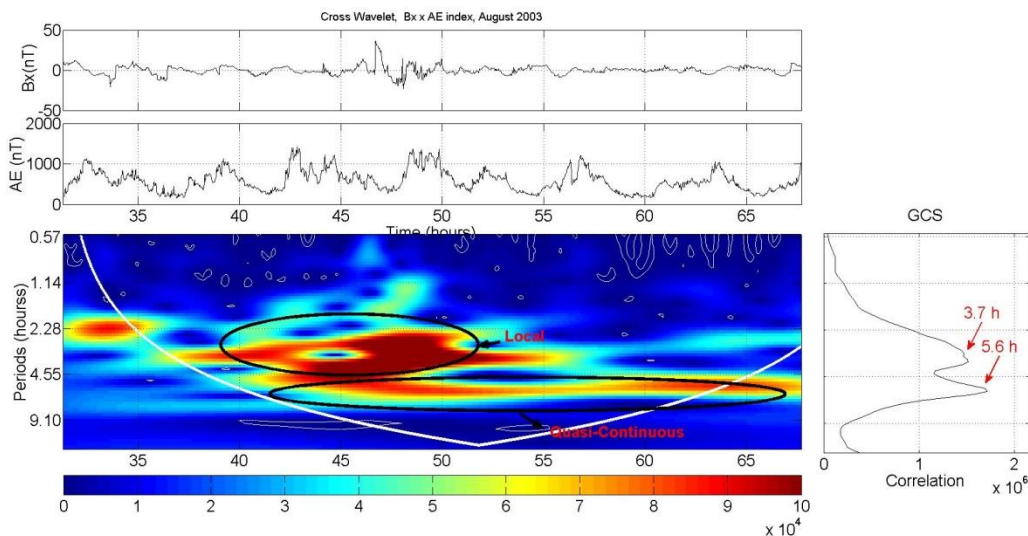


**Figure 7:** Histogram with the periods of highest correlations between Bz IMF component and Bx geomagnetic component.



5 Figure 8- a) Bx geomagnetic magnetotail component AE index time series; b) CWT for the HILDCAA event that occurred between 15:11 UT August, 20 and 15:43 UT August, 24, 2003. c) Global Correlation Spectrum.

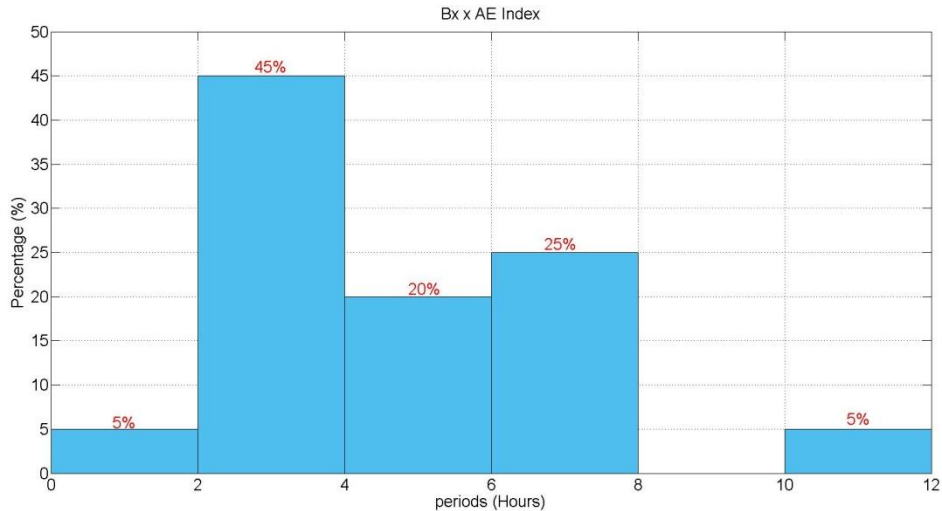


Figure 9- Histogram with the periods of high correlation between Bx tail component and the AE index.

5

10

15

20



## Tables

Table 1- Bx geomagnetic field component data information used for the HILDCAA events analysis in the magnetotail.

5 Table 2- Energy distribution classification of the geomagnetic component Bx during HILDCAAs.

Table 3- Correlation distribution characteristics between Bz-IMF and Bx geomagnetic component during HILDCAAs.

Table 4- Classification of the correlation distribution type between Bx geomagnetic tail field component and AE index  
During HILDCAAs.

10

15

20

25

30

35

40

45



Table 1- Bx geomagnetic field component data information used for the HILDCAA events analysis in the magnetotail

Event	Start HILDCAA	End HILDCAA	Duration of the Analyzed interval of the Cluster in the tail (hours and minutes)
1	2003-08-20/15:11 UT	2003-08-24 15:43 UT	36h 24 min
2	2003-09-15 21:02 UT	2003-09-20 22:03 UT	36h 24 min
3	2003-09-23 23:31 UT	2003-09-26 02:36 UT	36h 24 min
4	2003-10-15 03:38 UT	2003-10-22 18:35 UT	36h 24 min
5	2004-09-15 19:49 UT	2004-09-18 5:39 UT	42h 10 min
6	2005-08-05 22:19 UT	2005-08-07 22:59 UT	18h 12 min
7	2006-10-13 15:17 UT	2006-10-16 00:16 UT	18h 12 min
8	2006-10-28 14:15 UT	2006-10-30 16:27 UT	13h 14 min
9	2007-09-01 16:31 UT	2007-09-03 15:10 UT	13h 12 min

5 Table 2- Energy distribution classification of the geomagnetic component Bx during HILDCAAs.

Classification	Number of most energetic periods	Percentage (%)
Continuous	8	32
Quase-Continuous	6	24
Intermittent	7	28
Local	4	16



Table 3- Correlation distribution characteristics between Bz-IMF and Bx geomagnetic component during HILDCAAs.

Classification	Bx x Bz-IMF (GSM)	
	Number of periods	Percentage (%)
Continuous	1	4.3
Quasi-continuous	8	34.8
Intermittent	4	17.4
Local	10	43.5
(not Classified)	4	

5

Table 4- Classification of the correlation distribution type between Bx geomagnetic tail field component and AE index During HILDCAAs.

Classification	Number of periods of higher correlation	Percentage (%)
Continuous	1	5
Quasi-Continuous	7	35
Intermittent	1	5
Local	11	55